J Mater Sci (2010) 45:4770–4777
DOI 10.1007/s10853-010-4636-8

ULTRAFINE GRAINED MATERIALS

Hardness measurements of accumulative roll-bonded Mo foils

G. Marathe · R. J. Hebert

Received: 13 February 2010 / Accepted: 18 May 2010 / Published online: 5 June 2010

Abstract The hardness of accumulative roll bonding (ARB)-processed multilayers has been measured in the past with microindentation studies. In some cases the lateral indent size of microindenters, however, is too large. For example, if multilayers are ARB-processed that consist of arrays of different elemental foils the hardness ratio of the layers has been reported as a key factor for the development of diffuse necking. To predict diffuse necking during ARB processing, flow stress data are usually taken from tensile tests. Flow stresses can be estimated of individual layers based on hardness measurements. In this work results are compared between hardness measurements on ARB-processed Mo multilayers with micro- and nanoindentation. Two sets of Mo multilayers were examined, one with as-received Mo foils and a second set with annealed Mo foils as starting material. The microhardness measurements show an increase in hardness with the first two passes before the hardness reaches a near plateau for the annealed Mo foils. The as-received foils that appear to be cold-worked yield a constant hardness for the first five passes that approaches the hardness of the annealed samples after four passes. The nanoindentation measurements were conducted at the center of Mo grains. If the indentation size effect (ISE) is taken into account the nanoindentation-based hardness measurements of the annealed Mo foil multilayers agree with the microhardness measurements. For the multilayer comprised of as-received Mo foils, agreement is obtained with the microhardness measurements even without taking into account an ISE. These observations are discussed with respect to the changes in microstructural length scales during ARB processing and the indent sizes. A main conclusion is that nanoindentation measurements yield reliable hardness data if the ISE is considered.

G. Marathe · R. J. Hebert (✉)
Chemical, Materials, and Biomolecular Engineering Department, University of Connecticut, 97 N. Eagleville Rd., Storrs, CT 06269, USA
e-mail: rhebert@ims.uconn.edu

Introduction

Bulk nanostructured materials are defined as macroscopic solids with internal or microstructural length scales of less than 100 nm [1]. Two approaches are used to produce bulk nanostructured materials: (1) Top-down approaches whereby a coarse-grained bulk precursor material is processed until nanoscale microstructures develop. (2) Bottom-up approaches whereby atom by atom synthesis is used to build up bulk nanostructured materials [2]. Among the top-down approaches, severe plastic deformation (SPD) has developed into a processing approach for metallic materials with commercial impact. In SPD processing, large strains are applied to materials and the microstructures gradually reveal characteristic length scales at tens to hundreds of nanometers. Different approaches have been developed to impart large strains into materials, the most notable being equal channel angular extrusion, high pressure torsion pressing, and accumulative roll bonding (ARB). In ARB processing, sheet samples are repeatedly rolled and then folded or stacked to enable a cyclic process. Since cold rolling is a well-established sheet metal processing technique, ARB processing has quickly emerged as a popular SPD technique [3–12].

ARB processing has been applied to single-phase and multi-phase materials, often with very different objectives. While the ARB processing of single-phase materials aims mostly at grain-size reduction and the synthesis of bulk

nanostructured materials, the SPD processing of multi-phase materials has been applied not only to obtain nanostructured materials, but furthermore for driven alloying, i.e., the formation of new phases. The interest centered primarily on the synthesis of amorphous phases [13–18]. A common thread in ARB processing of multi-phase materials is the refinement in the size of the phases. In ARB processing of multilayer samples, for example, the individual layers decrease in thickness while at the same time their internal microstructures change simultaneously. The change in size and shape of the individual phases is a complex problem that depends on the mechanical properties of the starting material and the details of the rolling and folding process. A common observation is that the softer phases develop into a matrix phase and the harder phase or phases often develop plastic instabilities. The plastic instabilities can be recognized when shear bands develop or when individual layers develop necking behavior. The necking of individual layers is similar to necking of free-standing foils during tensile testing except that the layers in the multilayer are surrounded and bonded to adjacent metallic layers. The bonding between layers changes the necking behavior. While necking during tensile testing occurs at true strain values that numerically equal the strain-hardening coefficients, the onset of necking instabilities in multilayers has been observed to occur at higher strain values than the strain-hardening coefficient. A common view in the literature is that the onset of necking during a rolling process can be estimated from the flow stresses of the layers. A major challenge, however, is to determine the flow stresses of individual layers not only at the beginning of the ARB process, but more importantly during processing when it is not possible to isolate individual layers for tensile tests. The common approach has been, so far, to conduct tensile tests on the individual foils that comprise the multilayer, to fit the measured stress–strain data with empirical constitutive equations, and to use these equations to predict the onset of diffuse necking [19–22]. A main drawback of the current approaches to predict diffuse necking is indeed the extrapolation of the stress–strain data obtained from tensile tests to ARB-processed multilayers.

Flow and yield stresses can be determined not only from tensile tests but can be estimated from hardness tests [23–27]. A constraint factor is frequently used to relate hardness to the flow stress at a characteristic strain; the hardness is often taken as three times the flow stress [26]. For multilayers, the hardness of individual layers can be obtained from measurements on cross-sections. The layer thickness of rolled and folded multilayers, however, decreases rapidly and conventional microindentation hardness measurements are not suitable, since the lateral size of the indent on the cross-section quickly exceeds the individual layer thickness. If instead instrumented indentation techniques are used, hardness measurements can be conducted on individual layers as thin as 2 μm in cross-section. The main differences between the micro- and the nanoindentation approach are the applied load and the approach to determine the hardness. For nanoindentation measurements indent loads range between hundreds of microNewton and tens of milliNewton. Microhardness measurements are based on indent loads of hundreds of milliNewton to on the order of Newton. Hardness values are inferred from optically determined indent areas for microhardness measurements; the unloading curves of load–displacement curves are used in nanoindentation studies to determine hardness. The use of nanoindentation to determine the local hardness of individual phases, for example, layers of a multilayer sample, entails intriguing challenges. For small indentation depths that are necessary to probe phases with a lateral size on the analysis surface of the order of 1 μm, the indentation size effect (ISE) is one challenge, but it is a challenge that has been examined in some detail [28, 29]. The presence of boundaries near the indents poses further challenges. Boundaries occur at the interfaces between different layers and at the interfaces between grains. Indentation experiments have been conducted to determine the effect of grain boundaries on hardness based on Vickers hardness testing and based on instrumented indentation tests [30–36]. For ARB-processed samples, the microstructural length scales change during processing, adding to the complexity of the data evaluation. Previous work on Mo–Mo multilayers up to 25 rolling and folding passes showed a change in hardness thereby a change in flow stress of the individual element layers with deformation [37]. It was observed that the hardness of Mo–Mo multilayers dropped drastically after 10 roll-folding passes. This drop in hardness was attributed to the dynamic recovery effects that have been observed previously for Mo sheets [38]. The present work focuses on the early deformation stages in case of Mo–Mo multilayers, i.e., up to five rolling and folding passes. In contrast to the original ARB process [39], the rolling and folding process in the current work is conducted without heating of the elemental foils. The aim of this study is to determine and compare the hardness values based on nano- and microindentation studies. Microindentation-based hardness studies of ARB-processed samples have prevailed, so far, in the literature. The aim of the present work is to compare hardness measurements on Mo–Mo multilayers obtained from microindentation and nanoindentation measurements and to compare the indent sizes with the microstructural length scales. The results of the present study help determining the usefulness and limits of nanoindentation measurements for probing the hardness of individual layers in ARB-processed samples.

Experimental procedure

Molybdenum foils were used in this study with a purity of 99.95% purity and a starting thickness of the individual layers of 127 μm. For the rolling and folding process of as-received samples, three Mo layers were stacked and then folded once to obtain a sample made of six layers. It was this six-layer sample for the as-received condition that was then cold-rolled and folded. For the sample made of annealed Mo foils five foils were stacked initially and folded once prior to the rolling. The starting annealed sample thus contained a total of ten layers. The annealing process served to induce recrystallization and foils were annealed in vacuum at 1,200 °C for 10 h. The initial cleaning and degreasing of the molybdenum foils was followed by rolling and folding up to five passes at ambient temperature without using any lubricant on a two high electric rolling mill with 420 mm roll diameter. The rolled and folded samples were prepared for cross-sectional imaging by mechanical grinding on SiC papers up to #1200 grit size, final polishing using diamond suspension up to 1 μm followed by 0.3 μm Al_2O_3 and 0.06 μm colloidal silica in suspension. Microstructure analyses of ARB-processed molybdenum foils was conducted with optical microscopy, scanning electron microscopy (SEM) for layer thickness analysis, atomic force microscopy (AFM) for measuring pileups around nanoindents, and transmission electron microscopy (TEM). The thin electron transparent foils for TEM studies were prepared using electropolishing with 70% butanol + 20% perchloric acid + 10% methanol at 35 V and 15 °C. The instrumented indentation tests were conducted with a Nanoindentation XP (MTS Nano Instruments, Oakridge, TN) instrument with a Berkovich indenter using a 30-s hold time at full load. The raw data of the nanoindentation measurements was analyzed in one approach based on the Oliver–Pharr method [40] from single load measurements at a load of 5 mN. In a second approach, the ISE was determined based on multiload measurements. For each indent position, increasing loads were used of 5, 7, 10, and 15 mN. The holding time at the maximum load was 30 s. The final unloading segment was then corrected for thermal drift of the instrument at 10% of maximum load. The Nix Gao model [41] was applied to account for the ISE, i.e., the ISE-corrected hardness value H_0 was obtained from

$$H^2 = H_0^2\left(1 + \frac{h*}{h}\right).$$

For the multiload range used in the present work between 5 and 15 mN, the linear fit of the hardness data H^2, obtained from the Oliver–Pharr analysis, and the inverse of the indentation depth corrected for pile-ups yielded the ISE-corrected hardness.

Vickers microhardness measurements were performed with a load of 250 mN and a hold time of 15 s.

Results

The microstructure of the starting Mo foils is highlighted in Fig. 1. The as-received foils reveal a lamellar or pancake-shaped grain morphology depicted in Fig. 1a that is typical for cold-rolled sheets. The grain size is larger in the center of the sheet than at the surfaces as expected from the parabolic shear strain distribution in unlubricated rolled sheets. A bright-field TEM image of the starting as-received molybdenum foil is highlighted in Fig. 1b. The TEM image indicates the presence of dislocations in the grains as expected from the cold-worked condition of the as-received sheets. The grain size for the initial as-received Mo foil ranges from 500 to 1500 nm in the normal direction of the foil with the grain thickness of some center grains on the order of 5 μm. The length of the grains is between about 1 and 20 μm. Following annealing, the grain size is between 10 and 25 μm and many grains are nearly equiaxed as shown in Fig. 1c.

A key aspect of all SPD techniques is the dynamic, i.e., mostly athermal refinement of microstructures. In case of

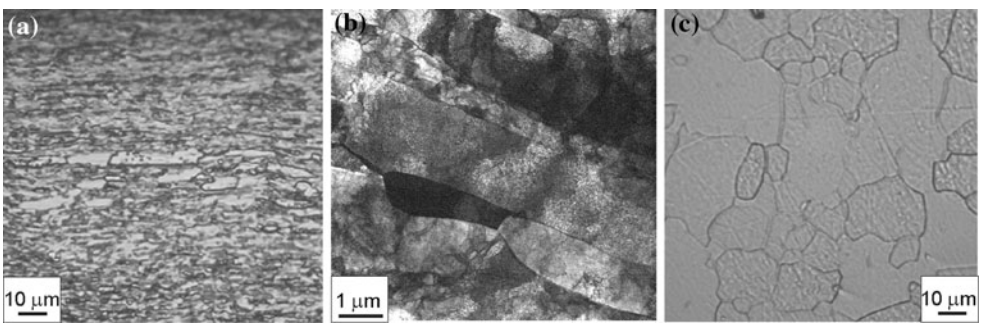

Fig. 1 **a** Optical micrograph of as-received Mo foil cross-section (127 μm thick). **b** Bright-field TEM image of as-received Mo foil (planar view). **c** Optical micrograph of annealed Mo foil

ARB processing, the main microstructural features that change length scales are the layer thickness and the grain size. Further microstructural changes are typically reflected in texture and grain shape. The average theoretical layer thickness after n rolling and folding passes for an initial layer thickness l_0 is $l = l_0/2^n$ if the reduction is assumed to be 50% per pass and under the assumption of plane strain deformation conditions. Figure 2 shows that the average layer thickness dropped more than 50% with each consecutive rolling and folding pass and reached 9 μm for both the annealed and as-received Mo foils. With a starting layer thickness of 127 μm, the average effective strain of the multilayer and the individual layers is −3.0. The simple scaling of the layer thickness that is suggested with the equation $l = l_0/2^n$ is not quite observed experimentally. Local sliding of the internal interface and incomplete overlap of the layers in the multilayer stack during folding can reduce the actual strain locally and induce a strain distribution [4]. Shear strains at the sample/roller interfaces moreover add to the effective strain and the shear contribution is not reflected in the simple layer thickness rule $l = l_0/2^n$. Nevertheless, the data presented in Fig. 2 does suggest a functional dependence between the layer thickness and the number of passes that can be described with an inverse power law relation.

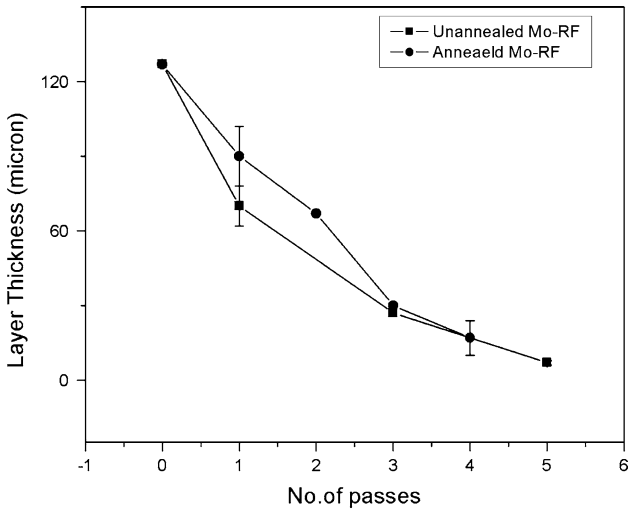

Fig. 2 Reduction in layer thickness with increasing number of rolling and folding passes

The grain size in the normal direction decreases simultaneously with the layer thickness while the grains elongate in the rolling direction. The reduction in grain thickness is highlighted in Fig. 3 for the annealed Mo foils. The annealed microstructure with the nearly equiaxed grains is shown in Fig. 3a. After the first rolling pass of a Mo–Mo multilayer the grains elongate in the rolling direction as shown in Fig. 3b and c. After four folding and rolling steps the individual layer thickness decreases to about 20–30 μm and one etched layer is depicted in Fig. 3c. The grain size in the layer normal direction can not be determined precisely from this image, but some grains are approximately 1–2 μm thick in the layer normal direction. Included in the optical micrographs and SEM images in Fig. 3 are schematic micro- and nanoindenter indents with the correct indent size relative to the grain sizes. The microindent size is approximately 14 ± 0.5 μm. Three-dimensional information about the nanoindent sizes can be gained from AFM. A nanoindent on a Mo foil with a diamond Berkovich indenter and a maximum load of 5 mN was analyzed with AFM and the lateral indent size of the nanoindent is 1.0 ± 0.25 μm as shown in Fig. 4. The indent depth is approximately 80 nm.

Figures 3 and 4 provide information about the relation between the number of rolling and folding passes and the microstructural features that can be probed with micro- and nanoindentation. For the annealed samples, the micro- and nanoindents can be placed within individual grains. Starting with the first pass, however, the microindent size approximately equals the size of the grains in the normal direction but is well below the thickness of an individual layer. With increasing number of ARB passes, microindentation becomes difficult to perform as the size of the microindent extends beyond the layer thickness especially after the second pass. For the second to fourth pass, the microindent increasingly exceeds the size of the grains in the normal direction but stays within the thickness of individual layers. For the fifth pass, however, the microindent is comparable

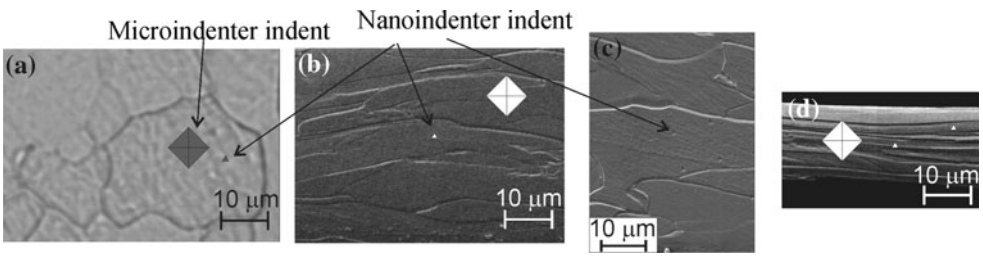

Fig. 3 Cross-sectional microstructure evolution of annealed Mo multilayer. **a** Annealed foil prior to rolling, **b** SEM image of cross-section after first roll pass, **c** first pass with array of nanoindents, **d** one layer in cross-section after five passes. Etching reveals grain structure

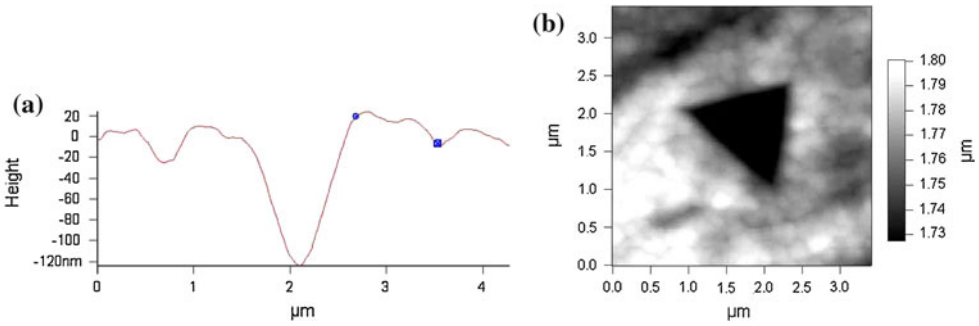

Fig. 4 **a** Profile of nanoindent at 5 mN load measured with AFM. **b** Topography of 5 mN nanoindent measured with AFM

to the size of the layer. For more than five roll and fold passes the microindent covers more than one layer and therefore in particular crosses layer boundaries. The nanoindents, on the other hand, can be placed not only within individual layers for the first five passes, but can be placed within individual grains of the initially annealed sample. Fig. 3c, for example, shows four indents that are located within one and the same grain after the first pass. For the as-received, un-annealed sample, both the nano- and microindents extend beyond individual grains from the beginning of the ARB process.

The hardness of the ARB-processed Mo-Mo multilayers was determined from micro- and nanoindentation studies. The results of the hardness measurements are depicted in Fig. 5 with respect to the number of roll and folding passes for annealed and as-received Mo-Mo multilayers. The difference between Fig. 5a and b is that only the Oliver–Pharr method was applied to the nanoindentation data for the graph in Fig. 5a while the ISE was taken into account in Fig. 5b for the nanoindentation data. The comparison between the two graphs in Fig. 5 shows that the hardness measured with instrumented indentation and with the Vickers hardness probe agrees to within their error ranges after the ISE is taken into account. If only the Oliver–Pharr analysis is applied, the hardness obtained from the nanoindentation data is significantly different from the Vickers hardness data in a sense that the error bars do not overlap.

The hardness data obtained in this study can be compared with the flow stress of Mo samples. A true stress–true strain diagram is depicted in Fig. 6 for an annealed Mo foil. For pyramidal indentors the representative or average strain is 8% [25]. The flow stress of the Mo foil at a true strain of 8% is about 824 MPa and hence a constraint factor is obtained of 2.73. By comparison, a constraint factor was reported for iron of 2.61. The hardness data obtained from the instrumented indentation and the microhardness measurements therefore not only agree to within 5%, but the hardness data corresponds to the flow stresses obtained from tensile tests.

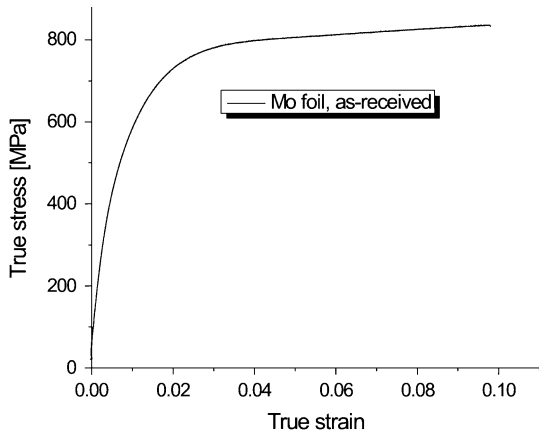

Fig. 6 True stress–strain curve for as-received Mo foil

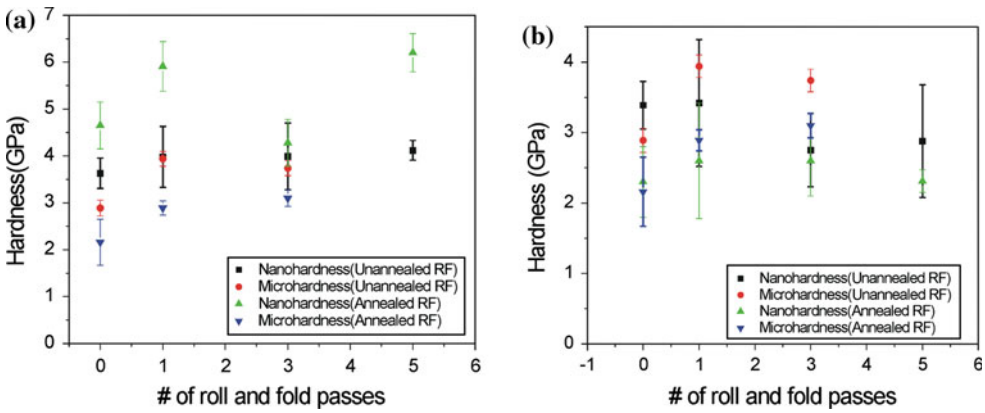

Fig. 5 **a** Hardness data obtained from micro- and nanoindentation measurements on ARB-processed multilayers for the first five passes. Nanoindentation data was analyzed with Oliver–Pharr method. **b** Hardness measurements of the same samples as measured in **a**, however, after applying Nix Gao model to account for indentation size effect

Discussion

Hardness changes during ARB processing

The results of the hardness studies reveal an increase in hardness for the multilayer with initially annealed Mo foils for the first two passes and a near constant hardness for up to five passes. This initial increase in hardness and leveling off at a plateau level has been reported for other SPD-processed materials [42–45]. The multilayer comprised of as-received Mo foils reveals a nearly steady hardness for the five roll passes studied in this work. The hardness of the multilayer with annealed foils approaches the hardness of the multilayer with the as-received foils after the first three to four roll passes. The plateau in hardness can be attributed to the saturation in the dislocation density with increasing number of roll-folding passes. While the focus of this work is directed toward the comparison between the nanoindentation and the microindentation hardness measurements it has been observed that for higher numbers of passes the hardness can increase from its plateau level. This behavior is highlighted in Fig. 7. In Fig. 7a hardness data is compiled of Mo–Mo, Mo–Ta, and Ta–Ta multilayers, each rolled and folded up to 25 passes and measured with microindentation. A key observation is that for 20 and 25 roll and fold passes the hardness of the Mo–Ta multilayer exceeds the hardness of the Mo–Mo and Ta–Ta multilayers. The cross-sectional microstructure of the Mo–Ta multilayer after 20 passes is highlighted in Fig. 6b; the layer thickness for both Mo and Ta layers is less than 1 μm and appears to be between about 500 nm and 1 μm. The increase in hardness for the Mo–Ta multilayer for these layer thicknesses points toward changes in the deformation behavior that could results from changes in the dislocation behavior such as confinement of dislocations within layers. Details of the high strain mechanical behavior are beyond the scope of this work, but it is clear that for layer thicknesses less than 1 μm the hardness analysis of individual layers based on nanoindentation measurements is very difficult due to effects that are discussed next.

Nanoindentation-based hardness measurement of ARB-processed multilayers

The main difference between the micro- and nanoindentation-based measurements is the size of the indent on the sample. For the 250 mN, used for microindentation in this study, the lateral size of the indent on the sample is about 12–14 μm. By contrast, the lateral indent size for a 5 mN load applied to the nanoindenter is about 1–1.5 μm as highlighted in Fig. 4. The indent sizes must be considered relative to the microstructural length scales. For the early stage of ARB processing, i.e., the first five passes for the current study the nanoindents have been placed at the center of grains for the multilayers with annealed foils. For the multilayers comprised of as-received foils the grain size in the normal direction to the rolling direction is from the beginning approximately equal or less than the size of the nanoindent and smaller than the microindent. Both measurements approaches therefore probe a sample volume that spans across grain boundaries. It must be taken into account that the relevant size in case of nanoindentation and to a lesser extent for microindentation is the plastic zone surrounding the indent and not the actual indent size. The interaction between the plastic zone and the grain size has been examined in [29, 34]. If the plastic zone is smaller than the grain size the hardness can be estimated if the ISE is taken into account for small indentation depths. In the current work this situation occurred for the multilayer comprised of annealed foils for the first five passes. As Fig. 5 demonstrates the hardness can be determined and agreement between nano- and microindentation hardness is obtained with the analysis based on the Nix Gao model. The plastic zone exceeds the grain size for the as-received grains for both analysis approaches. The results displayed in Fig. 5 demonstrate that in this case the hardness values

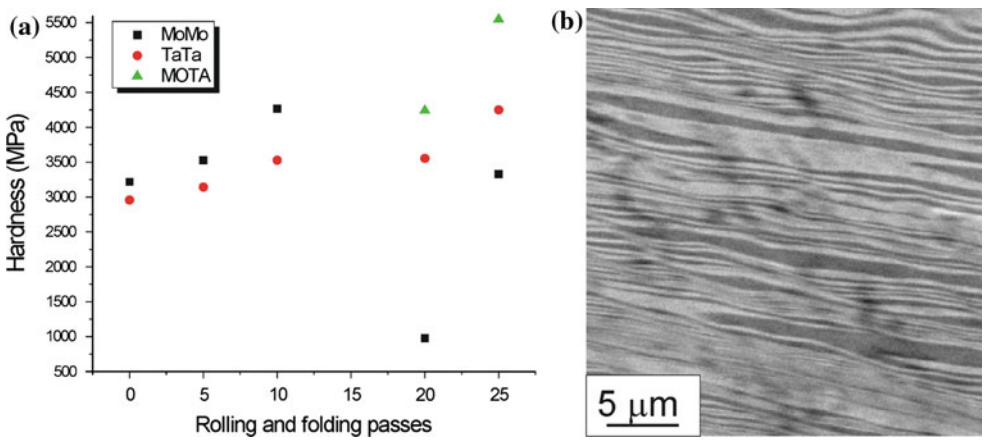

Fig. 7 **a** Hardness data for Mo–Mo, Mo–Ta, and Ta–Ta multilayers for up to 25 roll and fold passes. **b** Mo–Ta cross-sectional microstructure after 20 roll and fold passes

obtained from both approaches are within the error ranges after accounting for the ISE for the nanoindentation measurement.

The literature indicates that non-monotonic hardness changes can be observed with changes in the indentation depth due to a cross-over between the grain size and plastic zone length scales [34]. A non-monotonic behavior is observed in the current work for the nanoindentation measurement of the multilayers with unannealed Mo foils between the first and third roll pass and then the third and the consecutive roll passes. This behavior could be rationalized if the plastic zone of the indent was initially within a grain and then crossed the grain size after the first roll pass. In addition to grain boundaries, the layer boundaries represent another set of interfaces. Recent work demonstrated that nanoindentation measurements near boundaries or surfaces have to be corrected for the interaction between the plastic zone and the surface or boundary in addition to the ISE [30, 31]. Grain boundary hardening or softening has been examined on coarser length scales with microindentation studies [46]; the effects of grain or layer boundaries on the nanoindentation hardness analysis, which is clearly relevant for ARB-processed samples, requires further and more detailed examination that is currently underway.

The comparison between the strain at failure during the tensile test of the as-received Mo foil and the strain increase during the repeated rolling and folding highlights the strain range that can be analyzed with instrumented indentation tests on multilayer cross-sections. With an indent size of about 1 μm, the hardness can be assessed to a true strain of the individual layers of about four compared to a true strain at fracture of 0.08. In applying instrumented indentation measurements to determine hardness ratios between different layers it is important to take size effects and interactions between indents and layer boundaries into account. Instrumented indentation furthermore offers the opportunity to determine spatial variations in hardness across layers during the early stages of rolling and folding when the lateral indent size is small compared to the layer thickness. These spatially resolved hardness measurements will allow, for example, to determine if the current models for predicting the onset of diffuse necking in layers have to take the flow stresses near the layer boundaries into account or hardness values that are averaged over the layer thickness.

Conclusion

Local hardness and flow stress data is a main input for the prediction of necking in individual layers of rolled and folded multilayers. Instrumented indentation techniques can be used mainly for two purposes. The small indent sizes enable hardness measurements on individual layers to true strain levels on the order of 4 and therefore much higher strain levels can be analyzed than those accessible with tensile testing of individual layers. While indentation sizes on the order of micrometers allow for analyses of multilayers that have been rolled and folded several times, instrumented indentation techniques will be furthermore useful to detect spatial variations in hardness across layers at early deformation stages when the individual layers are typically on the order of tens to hundreds of micrometers thick. The current work demonstrates that for rolled and folded Mo–Mo multilayers Vickers hardness measurements and instrumented indentation techniques yield hardness values that agree within their error bars despite the very different nature of the two hardness measurements approaches. To obtain agreement, it is necessary to account for the ISE in the Mo layers. The refinement in grain- and layer sizes from the micrometer to the nanometer scale that is commonly observed during repeated rolling and folding provides for further opportunities to study nanoindentation in the presence of boundaries.

References

1. Gleiter H (1989) Prog Mater Sci 33:223
2. Zhu YT, Langdon TG (2004) JOM 56:58
3. Saito Y, Tsuji N, Utsunomiya H, Sakai T, Hong RG (1998) Scripta Mater 39:1221
4. Kamikawa N, Sakai T, Tsuji N (2007) Acta Mater 55:5873
5. Tsuji N, Saito Y, Seong-Hee L, Minamino Y (2003) Adv Eng Mater 5:338
6. Shaarbaf M, Toroghinejad MR (2008) Mater Sci Eng A 473:28
7. Eizadjou M, Kazemi Talachi A, Danesh Manesh H, Shakur Shahabi H, Janghorban K (2008) Compos Sci Technol 68:2003
8. Jiang L, Perez-Prado MT, Gruber PA, Arzt E, Ruano OA, Kassner ME (2008) Acta Mater 56:1228
9. Quadir MZ, Al-Buhamad O, Bassman L, Ferry M (2007) Acta Mater 55:5438
10. Acoff VL, Rengang Z (2007) Mater Sci Eng A 463:67
11. Dinda GP, Rosner H, Wilde G (2005) Mater Sci Eng A 410–411:328
12. Hoeppel HW, May J, Goeken M (2004) Adv Eng Mater 6:781
13. Atzmon M, Unruh KM, Johnson WL (1985) J Appl Phys 58:3865
14. Ben Ameur T, Yavari AR (1990) J Phys Colloq C4:219
15. Bordeaux F, Gaffet E, Yavari AR (1990) Europhys Lett 12:63
16. Bordeaux F, Yavari AR (1989) J Appl Phys 67:2385
17. Bordeaux F, Yavari AR, Desre P (1988) Mater Sci Eng 97:129
18. Hebert RJ, Perepezko JH (2003) Scripta Mater 49:933
19. Hwang Y-M, Hsu H-H, Lee H-J (1996) Int J Mach Tools Manuf 36:47
20. Nowicke F Jr, Zavaliangos A, Rogers HC (2006) Int J Mech Sci 48:868
21. Semiatin SL, Piehler HR (1979) Metall Trans A 10:85
22. Semiatin SL, Piehler HR (1979) Metall Trans A 10:1107
23. Cao Y, Xue Z, Chen X, Raabe D (2008) Scripta Mater 59:518
24. Umbrello D, Rizzuti S, Outeiro JC, Shivpuri R, M'Saoubi R (2008) J Mater Process Technol 199:64

25. Sundararajan G, Tirupataiah Y (1994) Bull Mater Sci 17:747
26. Tabor D (1951) The hardness of metals. Clarendon Press, Oxford
27. O'Neill H (1967) The hardness of metals and alloys. Chapman and Hall, London
28. Zong Z, Lou J, Adewoye OO, Elmustafa AA, Hammad F, Soboyejo WO (2006) Mater Sci Eng A 434:178
29. Durst K, Backes B, Goken M (2005) Scripta Mater 52:1093
30. Jakes JE, Frihart CR, Beecher JF, Moon RJ, Resto PJ, Melgarejo ZH, Suarez OM, Baumgart H, Elmustafa AA, Stone DS (2009) J Mater Res 24:1016
31. Jakes JE, Frihart CR, Beecher JF, Moon RJ, Stone DS (2008) J Mater Res 23:1113
32. Braunovic M (1973) In: Westbrook JH, Conrad H (eds) The science of hardness testing, its research applications. ASM, Metals Park, OH
33. Eliash T, Kazakevich M, Semenov VN, Rabkin E (2008) Acta Mater 56:5640
34. Yang B, Vehoff H (2007) Acta Mater 55:849
35. Soifer YM, Verdyan A, Kazakevich M, Rabkin E (2002) Scripta Mater 47:799
36. Goeken M, Kempf M, Bordenet M, Vehoff H (1999) Surf Interface Anal 27:302
37. Hebert RJ, Marathe G, Suri J (2009) In: TMS 2009. 138th annual meeting & exhibition. Supplemental proceedings: materials processing and properties, p 455
38. Dubovitskaya NV, Larikov LN, Bevza YV (1981) Phys Met Metall 51:154
39. Saito Y, Utsunomiya H, Tsuji N, Sakai T (1999) Acta Mater 47:579
40. Oliver WC, Pharr GM (1992) J Mater Res 7:1564
41. Nix WD, Gao H (1998) J Mech Phys Solids 46:411
42. Krallics G, Lenard JG (2004) J Mater Process Technol 152:154
43. Cherukuri B, Nedkova TS, Srinivasan R (2005) Mater Sci Eng A 410–411:394
44. Hosseini SA, Manesh HD (2009) Mater Des 30:2911
45. Eizadjou M, Manesh HD, Janghorban K (2009) J Alloys Compd 474:409
46. Westbrook JH, Conrad H (1973) The science of hardness testing and its research applications. American Society of Metals, Metals Park, OH